

Article

# Higher-Order Spectra Analysis-Based Diagnosis Method of Blades Biofouling in a PMSG Driven Tidal Stream Turbine <sup>†</sup>

Lotfi Saidi <sup>1,2</sup>, Mohamed Benbouzid <sup>2,3,\*</sup>, Demba Diallo <sup>3,4</sup>, Yassine Amirat <sup>5</sup>, Elhoussin Elbouchikhi <sup>5</sup> and Tianzhen Wang <sup>3</sup>

<sup>1</sup> Laboratory of Signal Image and Energy Mastery (SIME, LR 13ES03), Université de Tunis, ENSIT, Tunis 1008, Tunisia; lotfi.saidi@esstt.rnu.tn

<sup>2</sup> Institut de Recherche Dupuy de Lôme (UMR CNRS 6027 IRDL), University of Brest, 29238 Brest, France

<sup>3</sup> Engineering Logistics College, Shanghai Maritime University, Shanghai 201306, China; demba.diallo@geeps.centralesupelec.fr (D.D.); tzwang@shmtu.edu.cn (T.W.)

<sup>4</sup> Génie électrique et électronique de Paris (UMR CNRS 8507 GeePs), Université Paris-Saclay, CentraleSupélec, 91192 Gif-sur-Yvette, France

<sup>5</sup> Institut de Recherche Dupuy de Lôme (UMR CNRS 6027 IRDL), ISEN Yncréa Ouest, 29200 Brest, France; yassine.amirat@isen-ouest.yncrea.fr (Y.A.); elhoussin.elbouchikhi@isen-ouest.yncrea.fr (E.E.)

\* Correspondence: mohamed.benbouzid@univ-brest.fr

<sup>†</sup> This paper is an extended version of our paper published in the 2019 Annual Conference of the IEEE Industrial Electronics Society, Lisbon, Portugal, 14–17 October 2019; pp. 6998–7003.

Received: 30 April 2020; Accepted: 2 June 2020; Published: 5 June 2020



**Abstract:** Most electrical machines and drive signals are non-Gaussian and are highly nonlinear in nature. A useful set of techniques to examine such signals relies on higher-order statistics (HOS) spectral representations. They describe statistical dependencies of frequency components that are neglected by traditional spectral measures, namely the power spectrum (PS). One of the most used HOS is the bispectrum where examining higher-order correlations should provide further details and information about the conditions of electric machines and drives. In this context, the stator currents of electric machines are of particular interest because they are periodic, nonlinear, and cyclostationary. This current is, therefore, well adapted for analysis using bispectrum in the designing of an efficient condition monitoring method for electric machines and drives. This paper is, therefore, proposing a bispectrum-based diagnosis method dealing the with tidal stream turbine (TST) rotor blades biofouling issue, which is a marine environment natural process responsible for turbine rotor unbalance. The proposed bispectrum-based diagnosis method is verified using experimental data provided from a permanent magnet synchronous generator (PMSG)-based TST experiencing biofouling emulated by attachment on the turbine blade. Based on the achieved results, it can be concluded that the proposed diagnosis method has been very successful. Indeed, biofouling imbalance-related frequencies are clearly identified despite marine environmental nuisances (turbulences and waves).

**Keywords:** bispectrum; biofouling; diagnosis; spectral kurtosis; stator current; tidal stream turbine

## 1. Introduction

Nonlinearity is a crucial characteristic of power system signals, which can be used to highlight various physical behaviors, such as frequency interactions [1–5], interharmonic effects on power systems [5,6], incipient failures [2], noise cancellation [7], and phase coupling (PC) [3,4,7]. Several classical techniques for rotating asymmetry assessment such as imbalance and bending shafts

have been verified to work over the last few years [4,6–13]. In most cases, these conventional techniques do not take into account all the situations, as their application requires signal linearity and stationary hypotheses [14–19].

The main idea is that as these systems degrade, they tend to become more nonlinear, generating new frequency components [20–24]. These new frequencies are phase-coupled with the main (original) interaction frequencies; these phenomena are called nonlinear interactions (NITs). The PC correlation between the two interacting frequencies and the new frequency is the well-known quadratic phase coupling (QPC) and has been known as NIT “true” signature in dynamic systems [5,7,20,25,26]. Detection of QPC relationships presented in a signal is, therefore, a significant factor in understanding nonlinear physical systems such as power generation ones. Bicoherence, a standardized version of the bispectrum, is extensively used as an index of the QPC degree in the signal of interest [5].

Power spectrum density (PSD), dependent on Fourier Transform (FT), can be exploited to analyze signals in the frequency domain. Whereas FT is a linear analysis tool, it, however, does not contain any QPC information [27–32]. It is, therefore, not appropriate when considering NITs. In contrast to the PSD estimate, bispectrum has proven its usefulness as a powerful tool for detecting QPC associated with NITs. In [5,25], bispectrum or bicoherence has been used to analyze NIT when diagnosing and detecting faults in complex power systems.

In the last decade, higher-order statistics (HOS) has attracted much attention from research teams. For instance, it has been suggested a bearing fault diagnosis method called bispectrum-based empirical mode decomposition [4]. This method has been successfully applied for the analysis of induction machine vibration signals and NIT effects around the resonance frequency band. In this case, it has been claimed that an electromechanical system might have multiple natural frequencies that cover a vast frequency range. For example, a lower one may be in the 1–2 kHz range and a higher one may be over 5 kHz. In their case study, it just so happened that the second intrinsic mode function (IMF2) explained the very natural frequency that is strong and also strongly modulates (couples with) the bearing defect frequency. Depending on how high the data acquisition frequency is (e.g., 10 kHz, 20 kHz, or 50 kHz), the IMF2 might explain a lower or higher natural frequency that is weakly coupled with the bearing defect frequency. Thus, applying the proposed reduction noise method only to the first IMFs might give the best result. In [7], it has been recently proposed a theoretical and practical deterministic bispectrum-based context of coupled harmonics and its application to rotor fault diagnosis subjected to noise effects. However, there are remaining some problems to be dealt with, namely the selection of the theoretical formulation showing the noise cancellation when applying the bispectrum. In [9], signal bispectrum with various periodic components is considered. A diagnosis scheme, using a theoretical result, is then derived and proved to be efficient when applied for helicopter gearbox vibration signals. A new method using wavelet packet energy (WPE) as well as modulation signal bispectrum (MSB) investigation for gearbox fault diagnosis has been proposed in [10]. First, the raw vibration signals are turned into different time–frequency segments using wavelet packet decomposition (WPD), and then WPE is calculated in a one by one time–frequency segment. The MSB analysis is then applied to the reconstructed signal to achieve the fault characteristic frequency estimation for the gearbox failure diagnosis. In [11], a theoretical approach for an induction machine flux signal-based fault diagnosis is developed. In this case, the proposed approach was based on the sum of the bispectrum module mean value and the square value of the autocovariance function median. The achieved results seemed promising in discriminating between healthy and faulty states. An earlier study, carried out for reciprocating compressor failure diagnosis using motor current [12], has shown that random noise can be substantially removed with the MSB. MSB is a continuation of the common bispectrum for characterizing modulation signals as it conserves not just the main properties of HOS but also gives a sparse representation of complicated sidebands.

To the best of the authors’ knowledge, the QPC problem has been barely considered from the theoretical approach. In reference to the approach provided in [7,8], this paper aims to give a comprehensive account of the use of the bispectrum to reveal a possible QPC between frequency

components in stator current signals of a permanent magnet synchronous generator (PMSG)-based tidal stream turbine (TST) affected by an unbalance fault as a consequence of biofouling and under emulated wave and turbulence conditions.

Converting the huge power of oceans into reliable electricity is one of the great engineering challenges of our time. TST exploits the kinetic marine currents energy to produce electricity [15,16]. Underwater conditions such as high material corrosion, since the saltwater is so corrosive, marine biofouling (the creatures that attach themselves to anything submerged in the ocean) lead to degradation that requires an extra level of care and maintenance.

Hence, the purpose of the present work is the analysis and interpretation of the TST PMSG bispectra stator current subjected to imbalanced rotor blades caused by biofouling.

The rest of the paper is organized as follows. In Section 2, TST issues and challenges are first discussed. In Section 3, a general introductory context is provided to motivate the application of HOS as a signal processing tool. A discussion on the experimental results using bispectrum and spectral kurtosis analysis with theoretical proof are reported in Section 4. At last, Section 5 comes with a conclusion and prospective investigations.

## 2. Tidal Stream Turbine Challenges

Until now, the most used converters to harvest marine current energy are TSTs [17,23]. Tidal currents, as distinguished from many other sources of renewable energy, are a reliable form of kinetic energy produced by regular and periodical tidal cycles. Since tidal current energy production is not influenced by weather, it is predictable for hundreds of years in advance [17,23]. Thanks to the higher density of water, this explains that the blades can be smaller and rotate more slowly while producing a significant amount of power. Moreover, this natural predictability of tidal energy is very attractive for grid management, taking away the dependence on fossil fuel power plants. TSTs are mounted on the seabed at sites with high tidal and continuous ocean current velocities, where they capture energy from the flowing water.

Two main TSTs have been identified; horizontal axis as well as vertical axis TSTs, illustrated in Figure 1 [15,16]. Figure 2 depicts the severe environment in which TSTs operate. These systems are subject to random current waves and high turbulence effects produced from the irregular seabed. TSTs are designed to operate in high and variable marine current velocity sites where there is a huge amount of kinetic energy to be transformed into electricity [23]. This clearly highlights that TSTs will be subjected to very challenging conditions throughout their service life.



**Figure 1.** Sabella D10 (left) and Atlantis AR1500 tidal stream turbines (TSTs; right) [15].

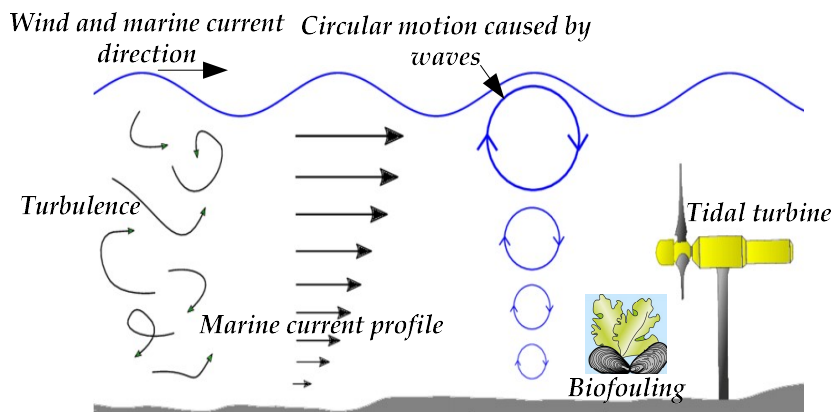


Figure 2. TST harsh environment conditions.

TSTs have an operational life of 25 years, with a maintenance cycle of five years [17]. During these long periods, due to harsh marine environmental conditions, such as high corrosion of materials, or marine biofouling due to an accumulation of microorganisms, plants, algae, and animals on immersed structures (Figure 3). This accumulation will often lead to mechanical imbalances, etc. (Figure 4). The above-mentioned factors imply frequent treatments and repairs, which are costly processes. Therefore, there is a strong need to reduce such monitoring as much as possible to improve the availability of TSTs. In [17], the main challenges for TSTs were reviewed and potential solutions were proposed, such as the use of alloy steel blades that avoid corrosion and have high structural strength. Research to address these challenges is still ongoing.



Figure 3. Biofouling attachment on a TST: (a) prior deployment, (b) TST retrieved from the ocean after some months [15,16].

TSTs condition monitoring is a challenging task of paramount importance due to systems offshore location and immersion conditions. In this regard, there is an obvious need for high reliability given the severe maintenance access limitations. In marine environmental conditions, biofouling can easily cause barriers and/or rise the weight and drag, thus substantially affecting the TST effectiveness [16]. Early detection of biofouling inception is one of the keys to improving TSTs reliability. In the available literature, attempts have been made to propose methods to diagnose TSTs rotor blade imbalances due to biofouling [13,14,16]. In such tidal stream energy harvesting systems, an imbalance fault typically induces cyclic impulses in the stator current. In this case, conventional time-series analysis is not

appropriate since impulses are most of the time buried in background noise or other undesirable frequency components [29,31]. To deal with this issue, advanced signal processing techniques are targeted.

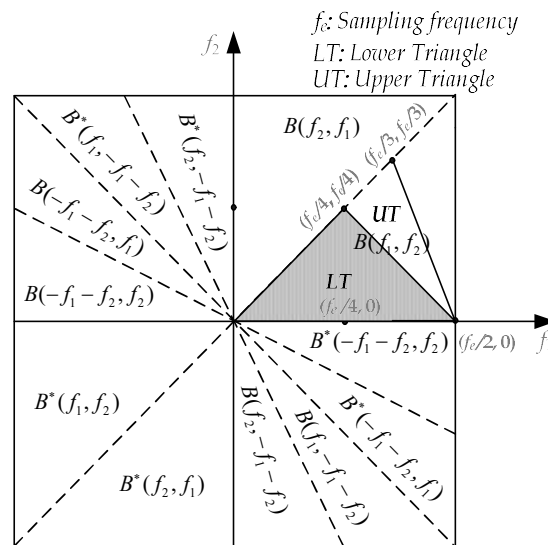


Figure 4. Bispectrum symmetry regions.

In this paper, the authors propose using HOS analysis to detect impulsive effect present in TST PMSG stator current signal, which is due to artificially created blades imbalance fault.

TST electrical signals are non-Gaussian and remarkably nonlinear [8,14,23]. Therefore, we suggest the use of HOS-based signal processing methods for the analysis and diagnosis of a TST experiencing blades imbalance caused by biofouling.

### 3. Higher-Order Statistics Analysis: Definitions and Properties

#### 3.1. Higher-Order Moments

In probability and statistics assumptions, the  $n$ -order central moment of a random variable  $X$  is determined as the expected quality of integer power,  $n$ , of the random variable  $X$  surrounding its mean, in accordance with the following formula [1,2]:

$$m_x^{(n)} = E\{(X - E\{X\})^n\} = \int_{-\infty}^{+\infty} (x - E\{X\})^n f_X(x) dx \tag{1}$$

where  $E\{\cdot\}$  indicates the expected value operator, superscript  $(n)$  defines the order of the central moment, and  $f_X(x)$  is the probability density function of  $X$ . Hence, the mean value is equal to zero,  $m_x^{(2)}$  and  $m_x^{(3)}$  represent the mean square value, and the mean cube value, respectively, and so forth.

HOS signal analysis involves a generalization of different order moments regarding a random variable to moment functions (i.e., correlation functions) about a random process. So, it is mathematically required to suppose that the random process has zero-mean for ease of computation. Under practical conditions, when handling real stator current data from monitored electromechanical systems, the signal mean is firstly computed and deduced from the signal.

Following the mathematical bases of HOS analysis, diverse order correlation functions may be calculated for the random process as listed below [1,2]:

$$\mu_x = E\{x(t)\} = 0 \text{ (or, a constant)} \tag{2}$$

$$R_{xx}(\tau) = E\{x^*(t)x(t + \tau)\} \tag{3}$$

$$R_{xxx}(\tau_1, \tau_2) = E\{x^*(t)x(t + \tau_1)x(t + \tau_2)\} \quad (4)$$

$$R_{xxx\dots}(\tau_1, \tau_2, \dots, \tau_n) = E\{x^*(t)x(t + \tau_1)x(t + \tau_2) \dots x(t + \tau_n)\} \quad (5)$$

where the superscript asterisk (\*) represents the complex conjugate. It is noticed that the second-order correlation function  $R_{xx}(\tau)$  is the well-known autocorrelation function. The third-order correlation function  $R_{xxx}(\tau_1, \tau_2)$  is often called a bicorrelation function. The fourth-order correlation function  $R_{xxxx}(\tau_1, \tau_2, \tau_3)$  is often called tricorrelation, and so forth.

When examining linear signals and systems, it is sufficient to consider Equations (2) and (3), which corresponds to a weakly stationary signal. For three harmonic signals interaction in a quadratically nonlinear situation as will be further addressed, a random signal is supposed to be stationary to the third-order (Equations (4) and (5)).

### 3.2. Power Spectrum

Power spectrum (PS) is a one-dimensional function of frequency and has been revealed to be highly potent in modeling linear physical problems. The discrete PS is the FT of the autocorrelation  $R_{xx}(\tau)$  [1,2,28–31] and can be estimated by

$$P_{xx}(f) = E\{X(f)X^*(f)\} = E\{|X(f)|^2\} \quad (6)$$

where  $X^*$  represents the complex conjugate of  $X$  and  $X(f)$  is the discrete FT of  $x(n)$ .

Since all information about the phase is discarded in computing the PS, it is unable to detect PC signatures.

### 3.3. Bispectrum and Bicoherence

Bispectrum, a third-order autocorrelation function  $R_{xxx}(\tau_1, \tau_2)$  2D FT, is performs well in detecting and quantifying QPC [1,2,28]. Meanwhile, it describes statistical links between signal frequency components. It is defined as

$$B(f_1, f_2) = E\{X(f_1)X(f_2)X^*(f_1 + f_2)\} \quad (7)$$

For the bispectrum to be nonzero at  $(f_1, f_2)$ , the FTs at frequency components  $f_1, f_2$ , and  $f_1 + f_2$  must be nonzero. Moreover, these three spectral components must be correlated. Note that, once the expectation is performed, the bispectrum will be zero owing to phase randomization and if phases are coupled it does not. Unlike the PS, even though the signal is real-valued, its bispectrum is complex.

The bispectrum symmetric regions are described in Figure 4 [1,2,28]. Therefore, the analysis can take into account just a single nonredundant region. In the following, throughout the paper,  $B(f_1, f_2)$  will designate the bispectrum in the nonredundant triangular region  $\zeta$  shown in Figure 4 in gray levels scale and described by;  $\zeta = \{(f_1, f_2): 0 \leq f_2 \leq f_1 \leq f_e/2; f_1 + f_2 \leq f_e/2\}$ , where  $f_e$  is the sampling frequency. Regions of computation are discussed in [1,2].

Therefore, bispectrum can be used to effectively solve several practical problems. Examples are expressed as follows [24–26]:

- If  $x(n)$  is a stationary zero-mean Gaussian process, its bispectrum is equally zero;
- While the PS deletes all phase information, the bispectrum does not.

The bispectrum is a quantified quantity of HOS. It is the FT of the third-order cumulant or moment. Nonlinearity affects these cumulants that are captured by the bispectrum.

The estimated bispectrum  $\hat{B}(f_1, f_2)$  is defined by

$$\begin{aligned} \hat{B}(f_1, f_2) &= \frac{1}{M} \sum_{k=1}^M X_k(f_1)X_k(f_2)X_k^*(f_1 + f_2) \\ &\approx E\{X(f_1)X(f_2)X^*(f_1 + f_2)\} \end{aligned} \quad (8)$$

The expectation operation is very significant in this situation and cannot be neglected mainly in QPC detection. It implies “ensemble averaging” for an estimate: if phases are random, the bispectrum tends to zero and if phases are coupled it does not.

The diagonal slice of the bispectrum (DSB) is a one-dimensional representation of the bispectrum by taking  $f_1 = f_2$ . This measure is given by [4,6,7]

$$\hat{B}(f_1, f_2)|_{f_1=f_2=f} = \hat{D}(f) \approx E\{X^2(f)X^*(2f)\} \tag{9}$$

The bicoherence or the normalized bispectrum in Equation (10) is a measure of the degree of QPC that appears in a signal or between two signals frequency components. As above-mentioned, PC is the estimate of the amount of energy in every potential pair of frequency components,  $f_1, f_2$ , which fulfills the definition of QPC (phase of the component at  $f_3$ , which is  $f_1 + f_2$ , equals phase of  $f_1 +$  phase of  $f_2$ ) [26,30]:

$$bic(f_1, f_2) = \frac{|B(f_1, f_2)|^2}{X(f_1)X(f_2)X(f_1 + f_2)} \tag{10}$$

when the analyzed signal reveals an arbitrary structure, PC can be expected to occur.

### 3.4. Bispectrum for Quadratically Nonlinear Systems

A characteristic of all nonlinear phenomena is the generation of “new” frequency components related to the sum and difference combinations of the “original” NIT frequencies [25,31,32]. These two frequencies (new and initial frequencies) must comply with a specific frequency selection rule that strongly depends on the order of the nonlinearity. Figure 5 shows a diagram of a general quadratic nonlinear system.

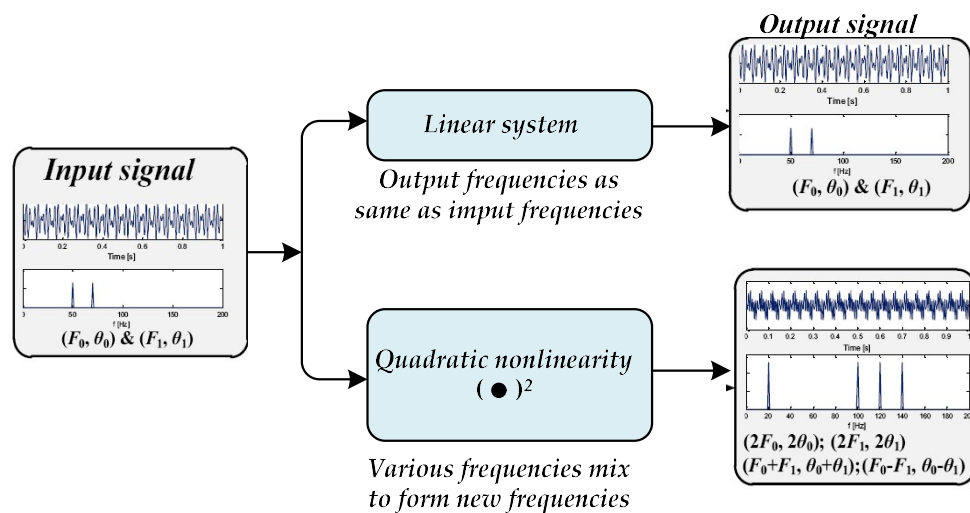


**Figure 5.** Diagram indicating the quadratically nonlinear interaction (NIT) between frequency components  $F_0$  and  $F_1$ .

Let us consider  $y(t)$  to be the output of the following nonlinear system

$$y(t) = x(t) + \epsilon x^2(t) \tag{11}$$

where the signal  $x(t)$  consists of two cosine waves at unrelated frequencies,  $F_0 = 50$  Hz and  $F_1 = 70$  Hz, with a sampling frequency of 512 Hz and contains 1024 samples. Parameter  $\epsilon$  denotes the nonlinearity coefficient.

Quadratic interaction implies the multiplication of two spectral components. Hence,  $y(t)$  can be rewritten in the form of harmonics using basic trigonometric formulas. These relationships are called QPC and are regarded to be a “true” signature of quadratic nonlinear systems [7,25,29]. Note that

harmonic random signals (Fourier series development of periodic signals) like those obtained from rotating machinery are not strictly stationary and are mainly cyclostationary. Their autocorrelation and higher-order correlations will be periodic [18–20].

In the output of this system, the signal will contain the components with frequencies and phases that are correlated (Figure 5). Such a phenomenon, which is characterized by these new phase relations, is called QPC and is highlighted by the bispectrum. The PS shows the distribution of the signal energy according to its frequencies. When this consideration is broadened to higher orders, the bispectrum offers information related to signal features such as phase coherence, which is lost in the second-order moment [1,2,24–28,30].

The bispectrum formula in Equation (8) indicates that, if the energy at the sum or difference of harmonic components is produced by a nonlinear process, phase coherence among the bifrequency components ( $F_0, F_1, F_0 + F_1$ ) appears and then the statistical average will indicate a nonzero value of the bispectrum result. This is an overall average for an estimate. Thus, if the phases are random, the bispectrum tends towards zero and if the phases are coupled, it is not the case.

Figure 6 considers the application of the bispectrum for QPC detection of the process in Equation (11) with  $F_0 = 50$  Hz,  $F_1 = 70$  Hz, and  $\varepsilon = 0.1$ . It should be noted the generation of second harmonics at 100 Hz, 140 Hz, and phase-coupled intermodulation components at  $F_0 + F_1 = 120$  Hz and  $F_1 - F_0 = 20$  Hz in the PS.

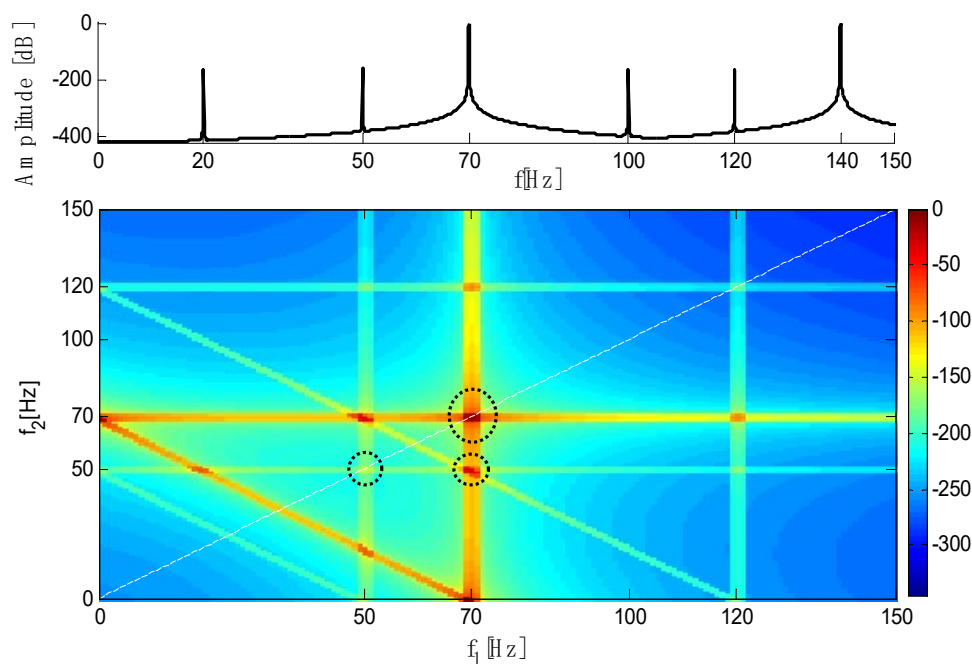


**Figure 6.** Power spectrum (PS; top panel) and bispectrum (bottom panel) of the nonlinear process given in Equation (11).

The associate bispectrum estimate arising from Equation (8) exhibits a peak at the bifrequency (70, 50) Hz. In practical applications, false peaks may occur in the bispectrum at points without any significant QPC resulting from several issues such as finite data length [7,31,32].

### 3.5. Bispectrum Gaussian Noise Cancellation

To evaluate the statistical behavior of the bispectrum in response to an additive white Gaussian noise (AWGN), we suppose that the noise  $n(t)$  is zero-mean Gaussian random variable ( $n(t) \sim \mathfrak{N}(0, \sigma_n^2)$ ). Its discrete FT is also a zero-mean Gaussian random variable ( $N(f) \sim \mathfrak{N}(0, \sigma_n^2/L)$ ). Where  $L$  is the number of discrete FT samples. Thus, the bispectrum becomes as follows:

$$\hat{B}(f_1, f_2) = E\{(X(f_1) + N(f_1))(X(f_2) + N(f_2))(X(f_3 = f_1 + f_2) + N(f_3)^*)\} \tag{12}$$

As we are focusing on coupled harmonics, the signal of concern generally contains sinusoidal components. Thus, the signal spectral component at particular frequencies can be expressed as magnitude and phase, for example,  $X(f_1) = A_1/2e^{j\theta}$ . Thus, the bispectrum in Equation (3) can be as follows:

$$\hat{B}(f_1, f_2) = E\left\{\left(\frac{A_1}{2}e^{j\theta_1} + N(f_1)\right)\left(\frac{A_2}{2}e^{j\theta_2} + N(f_2)\right)\left(\frac{A_3}{2}e^{j(\theta_1+\theta_2)} + N(f_3)^*\right)\right\} \tag{13}$$

Remembering that magnitude  $A$  and phase  $\theta$  of each sinusoidal frequency component are deterministic, then,  $E\{\cdot\}$  contributes only to noise components, which we will denote as  $N_1, N_2$ , and  $N_3$  for simplification purposes. Hence, Equation (13) can be reduced as follows:

$$\begin{aligned} \hat{B}(f_1, f_2) &= \left\{ \left( \frac{A_1 A_2 A_3}{8} \right) + E\{N_1 N_2 N_3^*\} \right\} \\ &+ \frac{A_1}{2} e^{j\theta_1} \frac{A_2}{2} e^{j\theta_2} E\{N_3^*\} + \frac{A_1 A_3}{4} e^{j\theta_2} E\{N_2\} + \frac{A_2 A_3}{4} e^{j\theta_1} E\{N_1\} \\ &+ \frac{A_1}{2} e^{j\theta_1} E\{N_2 N_3^*\} + \frac{A_2}{2} e^{j\theta_2} E\{N_1 N_3^*\} + \frac{A_3}{2} e^{-j(\theta_1+\theta_2)} E\{N_1 N_2\} \\ &\quad \downarrow \quad \quad \quad \downarrow \quad \quad \quad \downarrow \\ &= \frac{A_1 A_2 A_3}{8} + 0 + 0 + 0 + 0 + E_1 + E_2 + E_3 \end{aligned} \tag{14}$$

In Equation (14), first-order and third-order moments are then equal to zero,  $E\{N_1\} = E\{N_2\} = E\{N_3\} = E\{N_1 N_2 N_3^*\} = 0$ .

To quantitatively compare PS and bispectrum performance between, let us consider the signal  $x(t)$  given by the sum of three frequencies  $F_0 = 50$  Hz,  $F_1 = 70$  Hz, and  $F_2 = 120$  Hz in the presence of an AWGN  $n(t)$  with  $\sigma_{nx}^2 = 0.15$ , equivalent to 10 dB signal-to-noise ratio (SNR) defined by

$$SNR \triangleq 20 \log_{10} \left( \frac{\sigma_{x_n}^2}{\sigma_n^2} \right) \tag{15}$$

where  $\sigma_x^2$  is the variance of the signal  $x_n(t)$ .

Comparing power spectra results of Figures 7 and 8, it can be seen that signal frequency components are hidden in the noise making the PS more sensitive to noise compared to bispectrum.

Harmonic random signals such as those expected from PMSG-based TSTs are not strictly stationary and are cyclostationary in nature [19,20,25,27]. Their autocorrelation and higher-order correlations will be periodic. So, another way of the research can be extended to machine condition monitoring. Since the stator current signals of rotating machinery display a highly nonlinear and non-Gaussian behavior, bispectrum is then well appropriate to analyze this kind of signal.

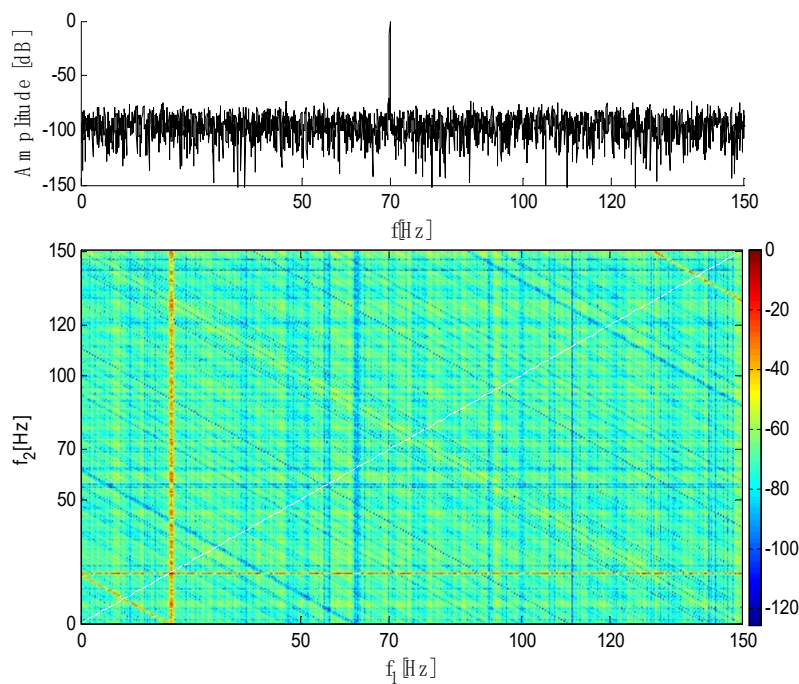


**Figure 7.** PS and bispectrum of the simulated signal  $x_n(t)$ , with additive white Gaussian noise (AWGN; signal-to-noise ratio (SNR) = 10 dB).

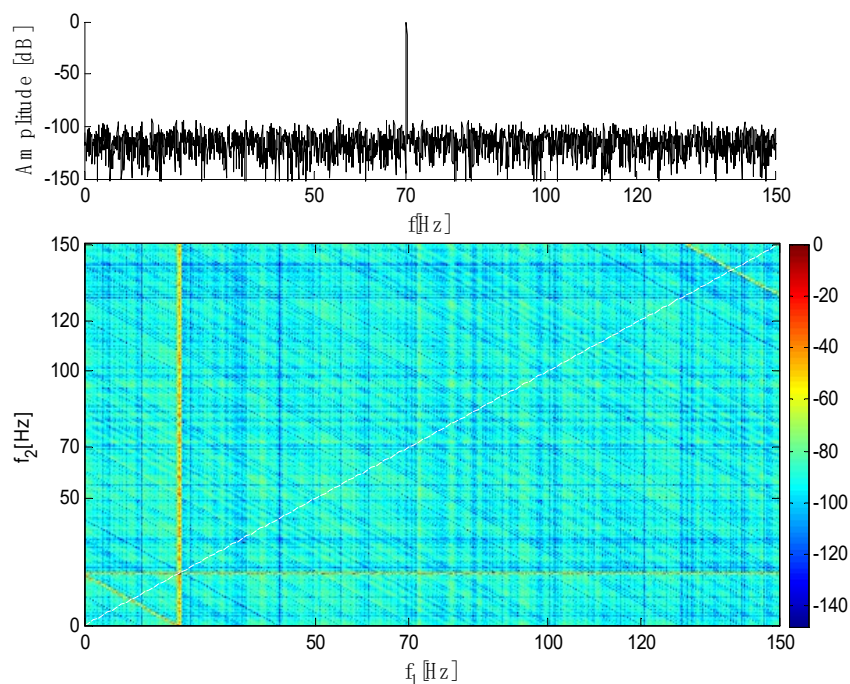


**Figure 8.** PS and bispectrum of the simulated signal  $x_n(t)$ , with AWGN (SNR = 20 dB).

#### 4. Tidal Stream Turbine Experimental Data-Based Tests

The proposed HOS-based biofouling diagnosis approach is tested on an experimental dataset issued from the Shanghai Maritime University TST platform. This platform consists of 230 W/8 pole pairs direct-drive PMSG-based TST operating in a water tunnel emulating waves and turbulences (Figures 9 and 10) [13,14]. Besides, 19 processing features were handled under varying operating conditions (wave and turbulence, Figure 11). The biofouling (imbalance fault) was emulated by attaching wire ropes on the rotor blade (Figure 10). Experimental data collection was made under the

following operating conditions: TST blades rotation was set at 120 rpm, the supply frequency  $f_s$  was around 15 Hz (actually 15.63 Hz), the data acquisition sampling frequency is 1 kHz, and the number of samples is 178,200.

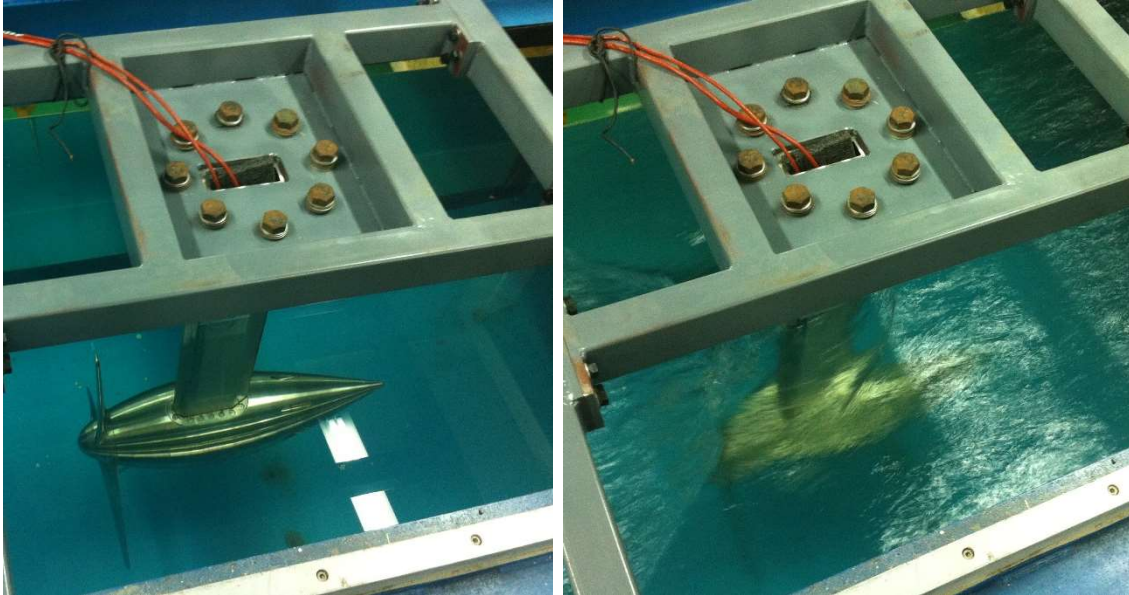


**Figure 9.** Permanent magnet synchronous generator (PMSG)-based tidal stream prototype into a water tunnel with illustration of turbulences and waves (left).



**Figure 10.** Imbalance fault (biofouling emulation) setting: healthy blade (left), imbalanced blade with 144 g attachment (right).

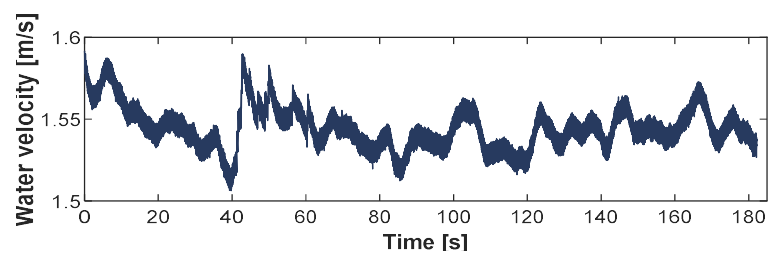


**Figure 11.** Adopted turbulent water velocity.

#### 4.1. PMSG Imbalanced Stator Current Model

Under rotor asymmetry, fault frequencies are determined by  $f_f = f_s \pm kf_r = (1 \pm k/p)f_s$ , where  $f_r$  is the rotational speed frequency,  $f_s$  is the supply frequency component,  $p$  is the pole pairs number, and  $k$  is an integer. With the blade imbalance fault, a simplified model, which describes the TST PMSG stator current, can be defined by [13,14]:

$$i_s(t) = A_t \cos(p\omega_m t + p\Delta\omega_m t + \varphi) \tag{16}$$

where  $A_t$  is the amplitude of the stator current,  $\varphi$  the initial angle,  $\omega_m$  is the PMSG shaft rotating speed, and  $\Delta\omega_m$  is the rotation speed variations.

$$i_s(t) = A_t \cos(\psi t + \varphi) \tag{17}$$

where  $\psi = p(\omega_m + \Delta\omega_m)$ .

The analytical signal of  $i_s(t)$  is  $\hat{i}_s(t) = A_t e^{j(\Psi t + \varphi)}$  and its FT is

$$I_s(\omega) = \frac{A_t}{2} \delta(\omega - \psi) e^{j\varphi} + \frac{A_t}{2} \delta(\omega + \psi) e^{-j\varphi} \tag{18}$$

where  $\omega = 2\pi f$  and  $\delta(\bullet)$  represents the Kronecker delta function.

By ignoring negative frequencies, Equation (18) can be written as:

$$I_s(\omega) = \frac{A_t}{2} \delta(\omega - \psi) e^{j\varphi} \tag{19}$$

Thus, each frequency component  $I_s(\omega_1), I_s(\omega_2), I_s(\omega_1 + \omega_2)$  produces one straight line in the  $(\omega_1, \omega_2)$  plane. For instance,  $I_s(\omega_1)$  will be represented by one line at  $\omega_1 = \psi$ . If  $I_s(\omega_1)$  is substituted from Equation (19) into Equation (8), the assigned bispectrum is equal to

$$\begin{aligned} \hat{B}(\omega_1, \omega_2) &= E\{I_s(\omega_1)I_s(\omega_2)I_s^*(\omega_1 + \omega_2)\} \\ &\approx \frac{1}{8} (A_t \delta(\omega_1 - \psi) e^{j\varphi}) \\ &\quad \times (A_t \delta(\omega_2 - \psi) e^{j\varphi}) \\ &\quad \times (A_t \delta(\omega_1 + \omega_2 - \psi) e^{-j\varphi}) \end{aligned} \tag{20}$$

From Equations (19) and (20), current  $i_s(t)$  bispectrum has nonzero values in lines intersection points on the  $(\omega_1, \omega_2)$  plane as shown in Equation (21) and in Figure 12.

$$\begin{cases} \omega_1 = \psi \\ \omega_2 = \psi \\ \omega_1 + \omega_2 = \psi \end{cases} \tag{21}$$

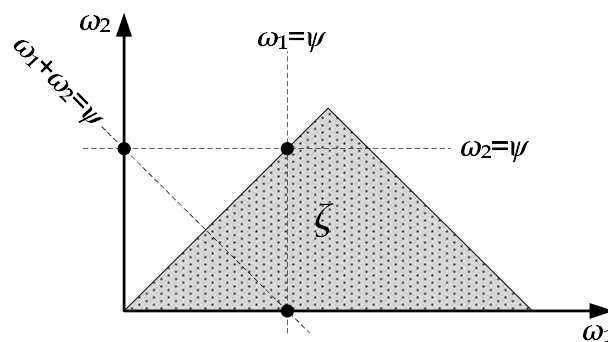


Figure 12. Theoretical bispectrum of TST PMSG stator current signal given in Equations (20) and (21).

4.2. Discussion

To demonstrate the effectiveness of the proposed bispectrum and its diagonal slice approach to detect rotor blade imbalance (with a QPC), both PSD and bispectrum are applied. Results are given in Figures 13–15. From Figure 13, we observe that the PSD is unable to identify any QPC information caused by the imbalance fault effect on the stator current.

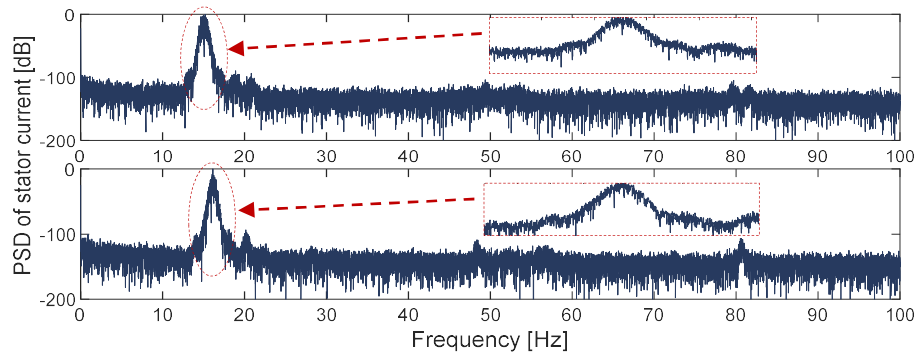


Figure 13. Stator current power spectrum density (PSD): healthy condition (upper PSD) and imbalanced rotor blades (lower PSD).

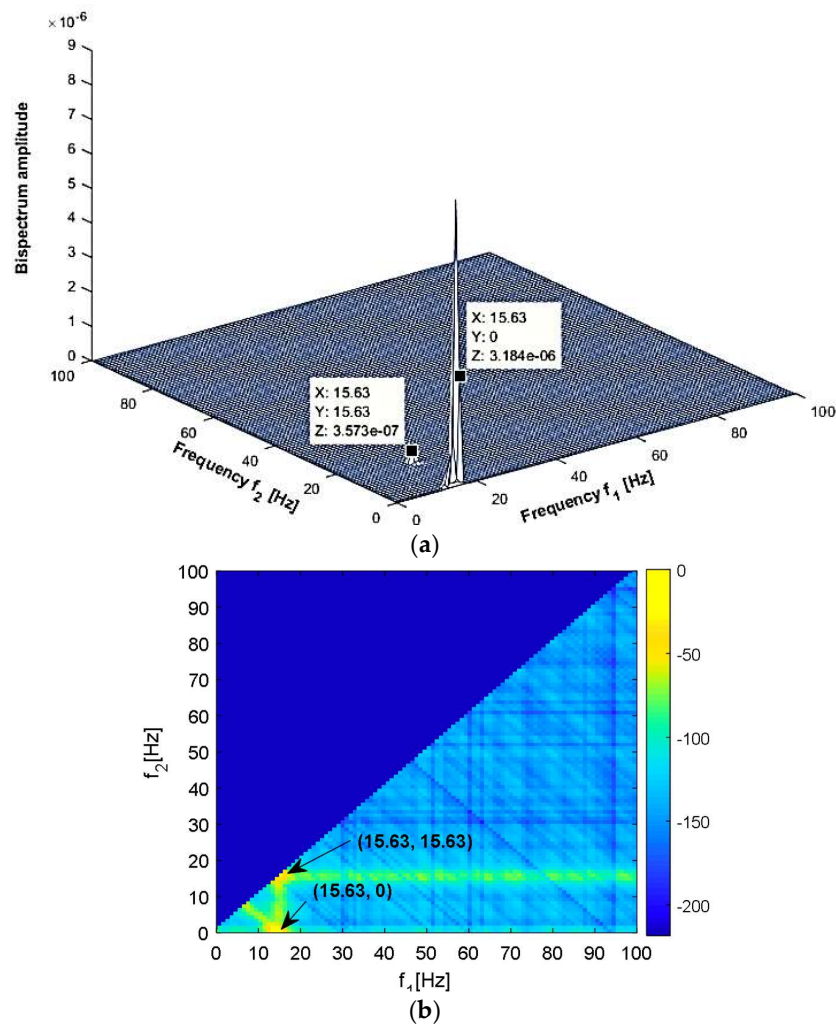
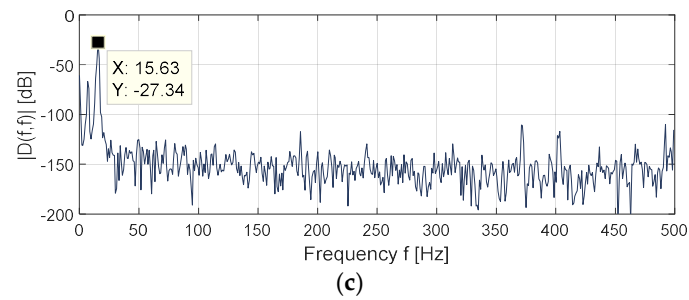
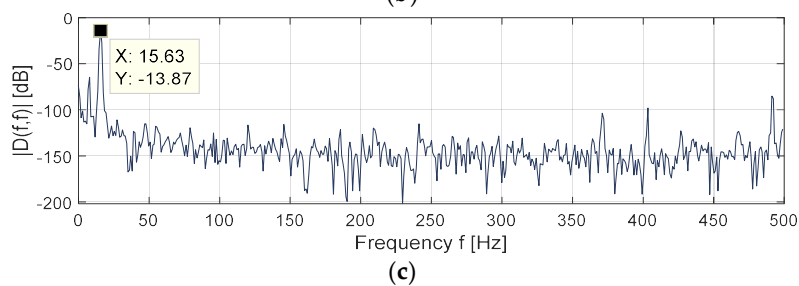
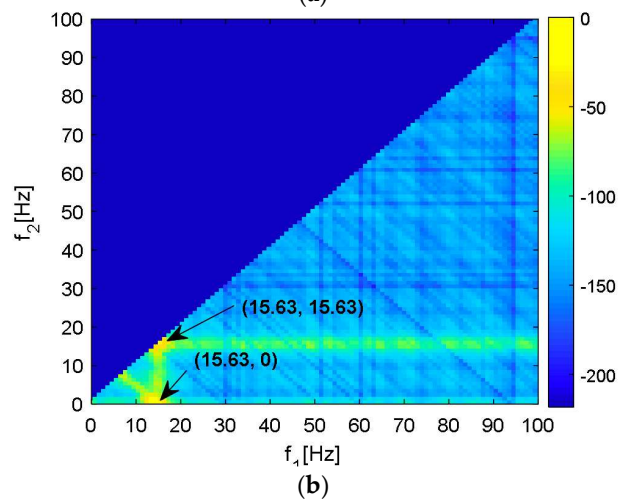
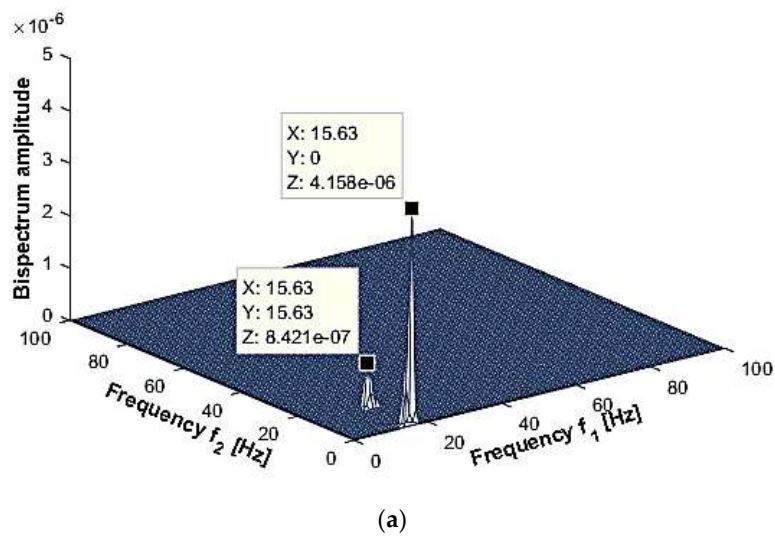


Figure 14. Cont.



**Figure 14.** TST PMSG stator current of the healthy rotor blades: (a) bispectrum, (b) normalized bispectrum amplitude, and (c) diagonal slice of the bispectrum (DSB).



**Figure 15.** TST PMSG stator current with imbalanced rotor blades: (a) bispectrum, (b) normalized bispectrum amplitude, and (c) DSB.

$B(f_s, f_s)$  is used as a condition indicator to distinguish between the faulty and the healthy blade states. The bispectrum magnitude response,  $B(f_s, f_s)$ , shows, in this case, its clear ability to detect the blade imbalance.

Further information can be retrieved from the same stator current data by expanding the analysis to the QPC behavior. The bispectrum magnitude is plotted for the same studied data set, as illustrated in Figures 14 and 15. The healthy example shown in Figure 14 has the least quadratic NIT frequency among the other cases. The highest bispectral peaks occur at the following coordinate bifrequency points:  $(f_s, 0)$ ,  $(f_s, f_s)$ .

In the rotor imbalance case revealed in Figure 15, increased frequency interaction along  $f_s$  frequency can be seen at the bifrequency coordinates  $(f_s, 0)$ ,  $(f_s, f_s)$ . An additional interesting observation is the high bispectral peak at  $(f_s, f_s)$  when compared with the healthy case. One can notice from the DSB of the faulty case, shown in Figure 15, that the peak amplitude is more than two times higher compared to the healthy case.

A deep insight into Equation (20) shows the presence of peaks in the bispectrum. Clearly, it can be identified by the nonzero products among the three terms of Equation (20). If the three  $\delta(\bullet)$  functions of each product have the same support, the result is nonzero and the related peaks occur in the bispectrum. From the experimental results shown in Figures 14 and 15, it can be seen the existence of two peaks located at  $(f_s, f_s)$  and  $(f_s, 0)$ , that corresponds to (15.63, 15.63) Hz and (15.63, 0) Hz.

In addition to the HOS- and PSD-based signal processing tools, the spectral kurtosis (SK) is a statistical tool, which can identify transient series and their positions in the frequency domain [17]. The fast kurtogram (FK) proposed in [18] is a benchmark method for fault detection [18–22].

The SK of a signal  $x(t)$  is given by [18]:

$$SK_x(f) = \frac{\langle |X^4(t, f)| \rangle}{\langle X^2(t, f) \rangle^2} - 2 \quad (22)$$

where  $\langle \bullet \rangle$  denotes the time–frequency averaging operator,  $X^4(t, f)$  and  $X^2(t, f)$  are respectively the fourth- and second-order spectral cumulants of  $x(t)$  band-pass filtered signal around  $f$ . Constant 2 is used since  $X(t, f)$  is the complex envelope of  $x(t)$  at frequency  $f$ .

From the SK definition in Equation (22), we can deduce:

- SK of a stationary process is a constant frequency function;
- SK of stationary Gaussian processes are similar.

However, the kurtosis value depends on both the central frequency  $f_c$  and the related bandwidth  $B_w$ . It is, therefore, difficult to define the decomposition mode [18–20]. In practice, several combinations of different central frequencies and bandwidths have to be tested to find an appropriate frequency band for signal envelope analysis, which requires extensive computations.

The achieved results are illustrated in Figure 16. The kurtogram is shown by Figure 16a, where the optimal bandwidth  $B_w$  and optimal carrier frequency  $f_c$  of the band-pass filter are set to 0.97 Hz and 15.63 Hz, respectively, while Figure 16b,c displays the filtered TST based PMSG stator current signal envelope spectrum and SK. As can be seen from Figure 16b, there is an apparent frequency impulse at the imbalance fault frequency (15.63 Hz) and its related harmonics, which suggests that the FK method can successfully identify the correct frequency resonance band and obtain the significant fault characteristic.

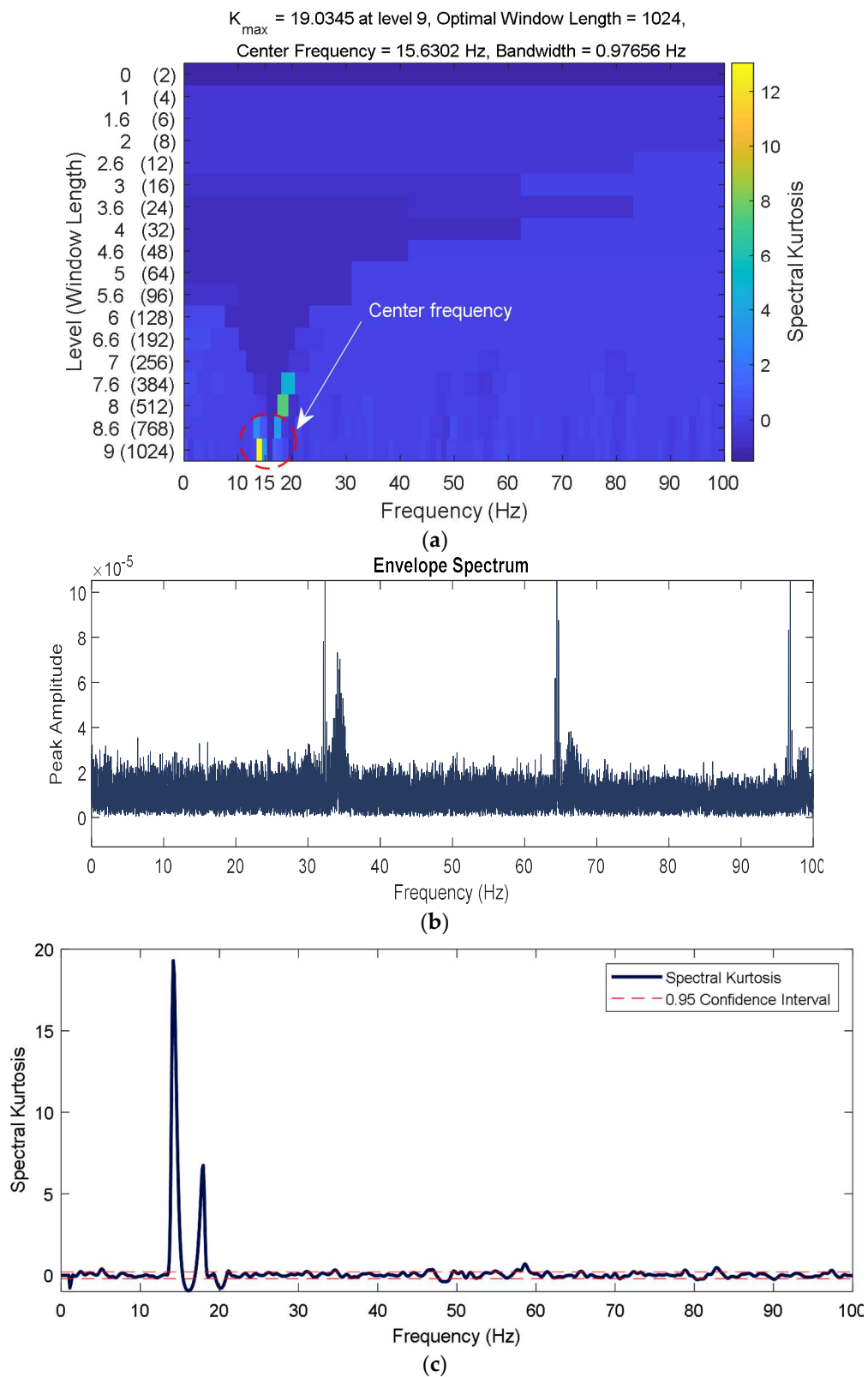


**Figure 16.** TST PMSG stator current with imbalanced rotor blades: (a) kurtogram; (b) envelope spectrum of the filtered signal, and (c) the spectral kurtosis (SK).

## 5. Conclusions

This paper has addressed the issue of diagnosing biofouling in tidal stream turbines. Biofouling is a natural process in marine environments that is responsible for turbine rotor unbalance. The proposed diagnosis method is based on the spectral representations of higher-order statistics, which describe statistical dependencies of frequency components that are ignored by conventional spectral measures. The bispectrum was adopted as studying higher-order correlations should provide more information on the tidal stream turbine condition.

The bispectrum was applied to the tidal stream turbine PMSG stator current. Based on experimental data, fault features were extracted offline and the achieved results seem to be encouraging compared to the classical power spectral density. The fault frequencies were identified despite the environmental nuisances due to noise and varying operating conditions (turbulence and waves).

Online tests should be further conducted to evaluate the accuracy of the proposed diagnostic approach and its computational cost.

**Author Contributions:** Conceptualization, L.S. and M.B.; Methodology, L.S., M.B., D.D., Y.A., E.E., and T.W.; Software, L.S.; Validation, L.S., M.B., D.D., Y.A., E.E., and T.W.; Formal Analysis, L.S., M.B., D.D., Y.A., E.E., and T.W.; Investigation, L.S. and M.B.; Writing—Original Draft Preparation, L.S. and M.B.; Writing—Review & Editing, L.S., M.B., D.D., Y.A., E.E., and T.W. All authors have read and agreed to the published version of the manuscript.

**Funding:** This research received no external funding.

**Conflicts of Interest:** The authors declare no conflict of interest.

## References

1. Nikias, C.L.; Petropulu, A.P. *Higher-Order Spectra Analysis a Nonlinear Signal Processing Framework*; Prentice-Hall: Enlewood Cliffs, NJ, USA, 1993.
2. Mendel, J.M. Tutorial on higher-order statistics (spectra) in signal processing and system theory: Theoretical results and some applications. *Proc. IEEE* **1991**, *79*, 278–305. [[CrossRef](#)]
3. Peng, Z.K.; Zhang, W.M.; Yang, B.T.; Meng, G.; Chu, F.L. The parametric characteristic of bispectrum for nonlinear systems subjected to Gaussian input. *Mech. Syst. Signal. Process* **2013**, *36*, 456–470. [[CrossRef](#)]
4. Saidi, L.; Ali, J.B.; Fnaiech, F. Bi-spectrum based-EMD applied to the non-stationary vibration signals for bearing faults diagnosis. *ISA Trans.* **2014**, *53*, 1650–1660. [[CrossRef](#)]
5. Messina, A.R.; Vittal, V. Assessment of nonlinear interaction between nonlinearly coupled modes using higher order spectra. *IEEE Trans. Power Syst.* **2005**, *20*, 375–383. [[CrossRef](#)]
6. Saidi, L.; Fnaiech, F.; Henao, H.; Capolino, G.; Cirrincione, G. Diagnosis of broken-bars fault in induction machines using higher order spectral analysis. *ISA Trans.* **2013**, *52*, 140–148. [[CrossRef](#)]
7. Saidi, L. The deterministic bispectrum of coupled harmonic random signals and its application to rotor faults diagnosis considering noise immunity. *Appl. Acoust.* **2017**, *122*, 72–87. [[CrossRef](#)]
8. Saidi, L.; Benbouzid, M.E.H.; Diallo, D.; Amirat, Y.; Elbouchikhi, E.; Wang, T. PMSG-based tidal current turbine biofouling diagnosis using stator current bispectrum analysis. In Proceedings of the IECON 2019—45th Annual Conference of the IEEE Industrial Electronics Society, Lisbon, Portugal, 14–17 October 2019; pp. 6998–7003.
9. Guoji, S.; McLaughlin, S.; Yongcheng, X.; White, P. Theoretical and experimental analysis of bispectrum of vibration signals for fault diagnosis of gears. *Mech. Syst. Signal. Process.* **2014**, *43*, 76–89. [[CrossRef](#)]
10. Guo, J.; Shi, Z.; Li, H.; Zhen, D.; Gu, F.; Ball, A.D. Early fault diagnosis for planetary gearbox based wavelet packet energy and modulation signal bispectrum analysis. *Sensors* **2018**, *18*, 2908. [[CrossRef](#)]
11. Iglesias-Martínez, M.E.; Antonino-Daviu, J.A.; Fernández de Córdoba, P.; Conejero, J.A. Rotor fault detection in induction motors based on time-frequency analysis using the bispectrum and the autocovariance of stray flux signals. *Energies* **2019**, *12*, 597. [[CrossRef](#)]
12. Gu, F.; Shao, Y.; Hu, N.; Naid, A.; Ball, A. Electrical motor current signal analysis using a modified bispectrum for fault diagnosis of downstream mechanical equipment. *Mech. Syst. Signal. Process.* **2011**, *25*, 360–372. [[CrossRef](#)]

13. Zhang, M.; Wang, T.; Tang, T. An imbalance fault detection method based on data normalization and EMD for marine current turbines. *ISA Trans.* **2017**, *68*, 302–312. [[CrossRef](#)]
14. Li, Z.; Wang, T.; Wang, Y.; Amirat, Y.; Benbouzid, M.; Diallo, D. A wavelet threshold denoising-based imbalance fault detection method for marine current turbines. *IEEE Access* **2020**, *8*, 29815–29825. [[CrossRef](#)]
15. Touimi, K.; Benbouzid, M.E.H.; Tavner, P. Tidal stream turbines: With or without a gearbox? *Ocean Eng.* **2018**, *170*, 74–88. [[CrossRef](#)]
16. Titah-Benbouzid, H.; Benbouzid, M.E.H. Biofouling issue on marine renewable energy converters: A state of the art review on impacts and prevention. *Int. J. Energy Convers.* **2017**, *5*, 67–78. [[CrossRef](#)]
17. Chen, L.; Lam, W.H. A review of survivability and remedial actions of tidal current turbines. *Renew. Sustain. Energy Rev.* **2015**, *43*, 891–900. [[CrossRef](#)]
18. Antoni, J. The spectral kurtosis: A useful tool for characterising non-stationary signals. *Mech. Syst. Signal. Process.* **2006**, *20*, 282–307. [[CrossRef](#)]
19. Barszcz, T.; Jabłoński, A. A novel method for the optimal band selection for vibration signal demodulation and comparison with the kurtogram. *Mech. Syst. Signal. Process.* **2011**, *25*, 431–451. [[CrossRef](#)]
20. Tian, X.; Gu, J.X.; Rehab, I.; Abdalla, G.M.; Gu, F.; Ball, A. A robust detector for rolling element bearing condition monitoring based on the modulation signal bispectrum and its performance evaluation against the kurtogram. *Mech. Syst. Signal. Process.* **2018**, *100*, 167–187. [[CrossRef](#)]
21. Saidi, L.; Ali, J.B.; Bechhoefer, E.; Benbouzid, M. Wind turbine high-speed shaft bearings health prognosis through a spectral kurtosis-derived indices and SVR. *Appl. Acoust.* **2017**, *120*, 1–8. [[CrossRef](#)]
22. Saidi, L.; Ali, J.B.; Benbouzid, M.; Bechhoefer, E. The use of SESK as a trend parameter for localized bearing fault diagnosis in induction machines. *ISA Trans.* **2016**, *63*, 436–447. [[CrossRef](#)]
23. Chen, H.; Tang, T.; Ait-Ahmed, N.; Benbouzid, M.E.H.; Machmoum, M.; Zaim, E.H. Attraction, challenge and current status of marine current energy. *IEEE Access* **2018**, *6*, 12665–12685. [[CrossRef](#)]
24. Nichols, J.M.; Murphy, K.D. Modeling and detection of delamination in a composite beam: A polyspectral approach. *Mech. Syst. Signal. Process.* **2010**, *24*, 365–378. [[CrossRef](#)]
25. Park, H.; Jang, B.; Powers, E.J.; Grady, W.M.; Arapostathis, A. Machine condition monitoring utilizing a novel bispectral change detection. In Proceedings of the 2007 IEEE Power Engineering Society General Meeting, Tampa, FL, USA, 24–28 June 2007; pp. 1–6.
26. Nichols, J.; Olson, C.; Michalowicz, J.; Bucholtz, F. The bispectrum and bicoherence for quadratically nonlinear systems subject to non-Gaussian inputs. *IEEE Trans. Signal Process.* **2009**, *57*, 3879–3890. [[CrossRef](#)]
27. Picinbono, B. Polyspectra of ordered signals. *IEEE Trans. Inf. Theory* **1999**, *45*, 2239–2252. [[CrossRef](#)]
28. Hinich, M.J.; Wolinsky, M. Normalizing bispectra. *J. Stat. Plan. Inference* **2005**, *130*, 405–411. [[CrossRef](#)]
29. Vasegh, S.V. *Advanced Digital Signal Processing and Noise Reduction*, 2nd ed.; John Wiley & Sons Ltd.: Hoboken, NJ, USA, 2008.
30. Wang, X.; Chen, Y.; Ding, M. Testing for statistical significance in bispectra: A surrogate data approach and application to neuroscience. *IEEE Trans. Biomed. Eng.* **2007**, *54*, 1974–1982. [[CrossRef](#)] [[PubMed](#)]
31. Priestley, M.B. *Nonlinear and Nonstationary: Time Series Analysis*; Academic Press: New York, NY, USA, 1988.
32. Barnett, A.G.; Wolff, R.C. A time-domain test for some types of nonlinearity. *IEEE Trans. Signal Process.* **2004**, *53*, 26–33. [[CrossRef](#)]

